Dynamic Functional Connectivity and Individual Differences in Emotions During Social Stress

Michael J. Tobia [1]* Koby Hayashi,[2] Grey Ballard,[2] Ian H. Gotlib,[3] and Christian E. Waugh[1]

[1]*Department of Psychology, Wake Forest University, Winston-Salem, North Carolina*
[2]*Department of Computer Science, Wake Forest University, Winston-Salem, North Carolina*
[3]*Department of Psychology, Stanford University, Stanford, California*

Abstract: Exposure to acute stress induces multiple emotional responses, each with their own unique temporal dynamics. Dynamic functional connectivity (dFC) measures the temporal variability of network synchrony and captures individual differences in network neurodynamics. This study investigated the relationship between dFC and individual differences in emotions induced by an acute psychosocial stressor. Sixteen healthy adult women underwent fMRI scanning during a social evaluative threat (SET) task, and retrospectively completed questionnaires that assessed individual differences in subjectively experienced positive and negative emotions about stress and stress relief during the task. Group dFC was decomposed with parallel factor analysis (PARAFAC) into 10 components, each with a temporal signature, spatial network of functionally connected regions, and vector of participant loadings that captures individual differences in dFC. Participant loadings of two networks were positively correlated with stress-related emotions, indicating the existence of networks for positive and negative emotions. The emotion-related networks involved the ventromedial prefrontal cortex, cingulate cortex, anterior insula, and amygdala, among other distributed brain regions, and time signatures for these emotion-related networks were uncorrelated. These findings demonstrate that individual differences in stress-induced positive and negative emotions are each uniquely associated with large-scale brain networks, and suggest that dFC is a mechanism that generates individual differences in the emotional components of the stress response. *Hum Brain Mapp 38:6185–6205, 2017.*

Key words: functional connectivity; tensor factorization; synchronization; stress; ventral PFC; temporal dynamics; positive affect; negative affect

INTRODUCTION

Emotions are an important and inseparable component of stress [Dickerson, 2008; Feldman et al, 1999; Folkman and Moskowitz, 2000; Lazarus, 1993; Tugade and Fredrickson, 2004], and successful cognitive performance depends on the ability to regulate emotional experience and neural activity during stress [Liston et al., 2009; Scheibe and Blanchard-Fields, 2009; Qin et al., 2009]. Several studies have examined functional connectivity of emotion networks during restful recovery from exposure to an acute psychosocial stressor [Soares et al, 2013; van Marle et al, 2010; Veer et al, 2012], but these studies neglect the importance of the temporal dynamics of emotions [Waugh et al.,

Additional Supporting Information may be found in the online version of this article.

Contract grant sponsor: National Institute of Mental Health; Contract grant number: MH80683; Contract grant sponsor: National Science Foundation; Contract grant number: 1642385

*Correspondence to: Michael J. Tobia, PhD; Wake Forest University, Department of Psychology, PO Box 7778, Winston-Salem, NC 27109, USA. E-mail: tobiamj@wfu.edu

Received for publication 28 July 2017; Revised 29 August 2017; Accepted 9 September 2017.

DOI: 10.1002/hbm.23821

Published online 20 September 2017 in Wiley Online Library (wileyonlinelibrary.com).

2015] during exposure to the stressor. In contrast to traditional functional connectivity, which refers to brain networks that are presumed to be stably synchronized, dynamic functional connectivity (dFC) refers to transiently synchronized (and desynchronized) networks, and can provide a time-resolved [Hutchison et al, 2013; Zalesky et al, 2014] perspective on the organization of brain networks during distinct phases of an acute psychosocial stressor, and during poststressor recovery. This study investigated dFC and individual differences in stress-induced subjective emotions in archival data [Waugh et al, 2012] of healthy human participants performing a social evaluative threat (SET) task while being scanned with functional magnetic resonance imaging (fMRI).

Temporal Dynamics of Emotions and Stress

Stressors disrupt homeostasis and well-being [Ulrich-Lai and Herman, 2009] through the coordinated activity of multiple brain systems for autonomic, endocrine and emotional regulation, and cognitive appraisal, action selection, and rumination [Hermans et al, 2014; Schultz and Vogele, 2015; Wager et al, 2009a; Wager et al, 2009b]. The component processes involved in emotions and stress make unique contributions and are not interchangeable [Mauss and Robinson, 2009], and each may unfold over their own unique behavioral and neural time scales [Moon and Lord, 2006; Verduyn et al., 2009, 2012; Lindquist et al., 2012; Esslen et al, 2004; Hot and Sequeira, 2013]. For example, appraisals are rapidly occurring processes, physiological arousal is much slower, and rumination occurs as a resurgence of emotional memories into consciousness after termination of the emotion eliciting stimulus. The neural responses associated with these emotional components also demonstrate different temporal dynamics, such as onset time, time to peak, duration, and resurgence after disengagement from the stressor [Waugh et al., 2012; Costa et al, 2014; Waugh et al., 2015]. Because different emotions and components of the stress response produce different neural dynamics, individual differences in subjective emotions during stress may be related to the dynamics of brain signals and large-scale brain networks.

Dynamic functional connectivity (dFC) allows for time-resolved analyses of network synchronization by computing functional connectivity over brief segments of time [Hutchison et al, 2013; Zalesky et al, 2014]. Studies employing dFC have shown that synchrony of large-scale brain networks is temporally unstable [Chang and Glover, 2010], although, whether this instability is due to true neural dynamics or some type of physiological or measurement noise, or randomness in signals, is currently debated [Handwerker et al, 2012; Hindriks et al, 2016; Laumann et al, 2016; Nikolau et al, 2016; Liegeois et al, 2017]. Nonetheless, numerous studies have identified a seemingly functional role for dFC in ongoing brain dynamics, either at rest [for a review, see Preti et al., 2017] or during task engagement [Gonzalez-Castillo and Bandettini, 2017]. From these studies, there is evidence that the brain reconfigures its topographical network organization on a moment-by-moment basis [Liegeois et al, 2016], and task-induced cognitive states, or other internal regulating factors such as mind-wandering, drive dynamic network reconfigurations [Braun et al, 2015; Mooneyham et al, 2017; Telesford et al, 2016]. Moreover, dFC captures individual differences in network dynamics [Xie et al., 2017], and several studies have demonstrated that dFC more strongly predicts behavioral characteristics compared to the presumed stable networks of functional connectivity computed over an entire time series [Jia et al., 2014; Jin et al, 2017]. Analysis of dFC group data, therefore, has the potential to reveal networks related to individual differences in subjective emotions.

Brain Regions Involved in Emotions and Stress

The ventromedial prefrontal cortex (vmPFC) is a key region associated with multiple components of emotional and stress processing including resilience to anticipatory threat and stress [van der Werff et al, 2013], and positive emotions [Winecoff et al., 2013; Wager et al, 2009a; Wager et al, 2009b; Roy et al., 2012]. Activation of the vmPFC is associated with greater self-reported stress, and it is involved in the relationship between cortisol regulation and subjective stress responsiveness [Wheelock et al, 2016]. Other research has shown that increased cortisol responsiveness is related to widespread limbic system deactivation including the vmPFC, hippocampus, ACC and hypothalamus [Pruessner et al, 2008]. Furthermore, the vmPFC is critical for successful emotion regulation through its effective connectivity with the amygdala [Motzkin et al., 2015; Morawetz et al., 2017].

Another important region in emotional and stress processing is the amygdala, which is associated with fear [Phelps and LeDoux, 2005] and uncertainty [Herry et al, 2007], but has also been shown to deactivate during a psychosocial stressor [Wager et al, 2009a]. Rather than activation or deactivation of the amygdala per se, functional connectivity between the amygdala and other brain regions is key to elucidating its role in emotion and stress processing. Functional connectivity between the amygdala and brain stem, and between the amygdala and the perigenual ACC, are both positively correlated with increases in stressor-evoked blood pressure [Gianaros et al, 2008]. Functional connectivity between the amygdala and vmPFC is important for successful emotion regulation [Banks et al., 2007; Motzkin et al, 2015; Morawetz et al, 2017], especially regulation of negative emotions [Urry et al, 2006]. Resting state functional connectivity between the amygdala and perigenual ACC, and between the amygdala and hippocampus, are correlated with cortisol regulation [Veer et al, 2012; Vaisvaser et al, 2013]. Exposure to an acute psychosocial stressor enhances subsequent resting

state functional connectivity of the amygdala with ACC, anterior insula and brain stem [van Marle et al., 2010], and the medial regions of the default mode network (DMN) [Veer et al, 2012].

The ACC is involved during both positive and negative emotion processing, as noted above, and the insula is associated with resilience to stress [Waugh et al, 2008]. The ACC is a central region of the intrinsically organized salience network [Seeley et al, 2007], which also includes the anterior insula. The salience network plays a role in interoception, the awareness of one's own bodily states, including visceral functions and pain. It is hypothesized to subserve the integration of internally and externally derived states, and coordinate further processing from other networks that determine which subsequent course of action may best serve the needs of the organism. The salience network is directly implicated in stress processing through an increased vigilance for negative emotional stimuli [Hermans et al, 2014], and salience network activity is correlated with self-report measures of anxiety (Seeley et al, 2007]. Together with the vmPFC and amygdala, the coordinated neurodynamics of the ACC and anterior insula, which are the core of the salience network, may be an important part of large-scale network synchronization in response to acute psychosocial stress.

The research reviewed above emphasizes the importance of temporal dynamics when investigating neural correlates of emotion and stress, and documents that the vmPFC, amygdala, ACC, and anterior insula (i.e., salience network), cooperate to process various components of emotions and stress. As such, individual differences in stress-induced subjective emotions may be related to dFC of brain networks involving these regions. Few studies in the literature on emotions and stress have investigated the dynamics of within network synchronization during acute psychosocial stress [Cribben et al., 2013], and most studies instead have focused on recovery from a stressor during a resting state [van Marle et al., 2010; Veer et al, 2012; Vaisvaser et al, 2013; Soares et al., 2013]. The main objective of this study was to assess whether individual differences in subjective emotional experience induced by an acute psychosocial stressor are reflected in the dFC of large-scale brain networks across healthy participants, whether these networks involve connectivity with the vmPFC, amygdala, and salience network, and if their functional connectivity fluctuates, or is fixed (i.e., idle) over time, during different stages of the SET.

METHODS

Participants

Sixteen healthy adult females participated in the fMRI experiment. Participants had no history of psychological or psychiatric illness, and no history of substance abuse. The participants were 25–45 years old (mean[sd] age = 33.64[9.36] years). Additional information about the participants and other data have been previously reported in Waugh et al. [2012] as the healthy control group, but the analyses conducted and reported here are independent of those previously reported.

Social Evaluative Threat (SET) Task

Participants performed an SET stressor task while being scanned with fMRI. The SET task involves preparation of an impromptu speech to be delivered to, and evaluated by, a panel of expert judges. It is an effective stressor that elicits anticipatory threat, and is associated with emotional, cardiovascular, respiratory, neuroendocrine, and neural responses [Bosch et al, 2009; Dickerson, 2008; Waugh et al, 2012; Waugh et al, 2010; Wager et al, 2009a; Wager et al, 2009b; Smith et al, 1997; Cavanaugh and Allen, 2008].

The SET is a continuous 7 min and 30 s scan composed of 5 phases: (1) resting baseline period (2 min); (2) task instruction period (1 min 20 s); (3) speech preparation period (2 min); (4) stress relief prompt (10 s); and (5) rest/recovery period (2 min). During the task instruction period, participants were informed they had 2 min to prepare a 7-min speech communicating "why you are a good friend," and that they would have to deliver their speech to an audience who would evaluate them after the scanning session. In the speech preparation period, participants were instructed to "prepare your speech now," which remained on the screen for the entire period until the relief prompt was presented. The participants had no prior knowledge of the speech task or topic. At the relief prompt, participants were informed that a coin flip had determined they would not give their speech (relief), which was followed by 2 min of restful recovery. In the recovery period, participants were instructed to wait for the next task to begin. Throughout this period, participants viewed a fixation cross. All instructions were visually presented, and participants completed the task with their eyes open.

While the SET contains several distinct periods demarcated by the presentation of visual stimulus events, it is best characterized by covert mental events, such as speech preparation and rehearsal, or emotion-related thought intrusions that may exacerbate or mitigate the effects of the threat as a stressor. Due to the covert mental nature of these types of events, their timing relative to the scan, including onsets, durations, and periodicities, are hidden from the experimenter and therefore unknown. This presents a challenge for elucidating the neural mechanisms of stress and coping that are involved in the SET, but the method of analyzing dFC described below was designed to address these challenges.

Retrospective Self-Report Ratings of Emotional Intensity

After scanning, participants completed a short questionnaire [see Waugh et al., 2012 for a full description of the

questionnaire] retrospectively assessing positive and negative emotions for two specific SET events: (1) when they learned about the speech task (threat) and (2) when they learned they would not have to give the speech (relief). The questionnaire included self-report ratings for each of 12 feelings (proud, distressed, excited, upset, strong, relieved, irritable, scared, inspired, nervous, determined, and enthusiastic) that fall into two categories: positive and negative emotions. Participants rated themselves on these feelings using a scale from 1 to 5, where a rating of 1 corresponded to "not at all" and a rating of 5 corresponded to "a great deal." For each emotion category, the ratings are averaged together to obtain a summary measure of positive and negative emotional intensity. The emotion ratings were completed twice in succession, always ordered for feelings about the stressor, followed by feelings about relief from the stressor.

MR Data Acquisition and Processing

MR data were acquired on a 3 T GE whole-body scanner with an 8-channel head coil. Structural images were acquired with a T1 MPRAGE pulse sequence. Functional images included 225 T2*-weighted gradient echo echo planar imaging volumes (31 slices, TR = 2000 ms, TE = 40 ms, 3.5 × 3.5 × 4 mm voxels) with a spiral sampling of k-space to reduce artifacts. Data were processed with a combination of AFNI [Cox, 1996] and custom Matlab code. The functional image time series were corrected for slice timing offsets and interscan head movement, and then smoothed with an 8 mm FWHM Gaussian kernel. The anatomical T1-weighted image was aligned to the mean of the functional images for each participant, and then transformed to MNI standard space. The smoothed functional image time series were then warped to MNI space using the parameters obtained from the warped T1-weighted image, with a spatial resolution of 4 mm isotropic voxels. The effects of head movement (6 rigid body parameters) and the average time course from an eroded white matter mask were removed from the functional time series by linear regression. The mean time course from each of 200 regions-of-interest (ROI) defined by a functional parcellation [Craddock et al, 2012] were obtained and used for dFC analyses. This parcellation provides reasonable spatial resolution to cover the whole-brain while reducing the computational burden of voxel-wise dFC analyses. Anatomical labels for the Craddock 200 parcellation are derived from the Harvard-Oxford Atlas with 112 distinct cortical and subcortical labels.

Dynamic Functional Connectivity

A common approach to dFC is sliding window functional connectivity (SWFC), which is computed as the Pearson correlation coefficient over a series of time segments between pairs of signals. SWFC has drawbacks related to limited temporal resolution that obscure brief events or cause spurious correlations [Leonardi and Van De Ville, 2015; Shakil et al., 2016]. Alternatively, the relative phase of two narrow band signals, referred to as instantaneous FC (iFC), yields a synchronization coefficient for each time point, and has been applied as a measure of dFC in resting state and passive sensory stimulation fMRI research [Glerean et al., 2012; Ponce-Alvarez et al., 2015; Senden et al., 2016]. However, the iFC requires a narrow frequency bandwidth prior to performing a Hilbert transformation to obtain phase vectors, which may limit its applicability for task-based dFC studies, especially when the temporal characteristics of events are unknown (i.e., onsets, durations, periodicities) as in the SET. Panel B of Figure 1 illustrates the iFC for the pair of wideband fMRI signals shown in panel A. Frequency modulations from the wideband signals in the phase vectors obtained via the Hilbert transformation corrupt the iFC (computed as the cosine of the relative phase of two signals) and create rapid fluctuations between synchronized and anti-synchronized states, making it unsuitable for analyses when events and event timing is unknown.

To investigate dFC in the SET in which the timing of events is unknown, we developed a filter that is applied to the iFC to eliminate rapid dynamics, which yields a smooth dynamic connectivity signal (DCS). The DCS is an intrinsic (parameter free) lowpass filter extracted from the iFC (computed from wide band signals) as a trace of the point-wise mean of the upper and lower envelopes of the iFC. It is essentially the opposite of the signals obtained from the empirical mode decomposition [Huang et al, 1998]. Whereas the empirical mode decomposition returns oscillatory signals, the DCS returns the non-oscillating signal transients. Figure 1 illustrates the procedure for calculating the DCS and compares it with the iFC and two SWFC time courses. Figure 1C shows the DCS within the iFC envelope, and demonstrates that extreme fluctuations in the iFC are almost completely nullified. The upper and lower envelopes are obtained by interpolating between the positive and negative peaks of the iFC, respectively. Figure 1D shows the DCS in comparison to SWFC with windows of 16 or 32 time points (i.e., 32 and 64 s, respectively). The DCS ranges from 1 to −1 for strong synchronization and anti-synchronization, respectively, and 0 for unstable/no synchronization. Figure 2 illustrates that the DCS filter nullifies the effects of frequency modulations, phase crossings, and phase resetting in wideband signals, and still provides maximal temporal resolution relative to the sampling rate.

Group Analysis and Tensor Decomposition

The DCS was computed for each pair of the 200 time courses, resulting in a 225 × 200 × 200 (time × ROI × ROI) connectivity tensor for each participant. This tensor contains a symmetric matrix of the DCS of each pair of the 200 ROIs at each of the 225 time points from the scan. Group-level analysis was conducted by concatenating the DCS tensor of each participant ($N = 16$), yielding a 225 ×

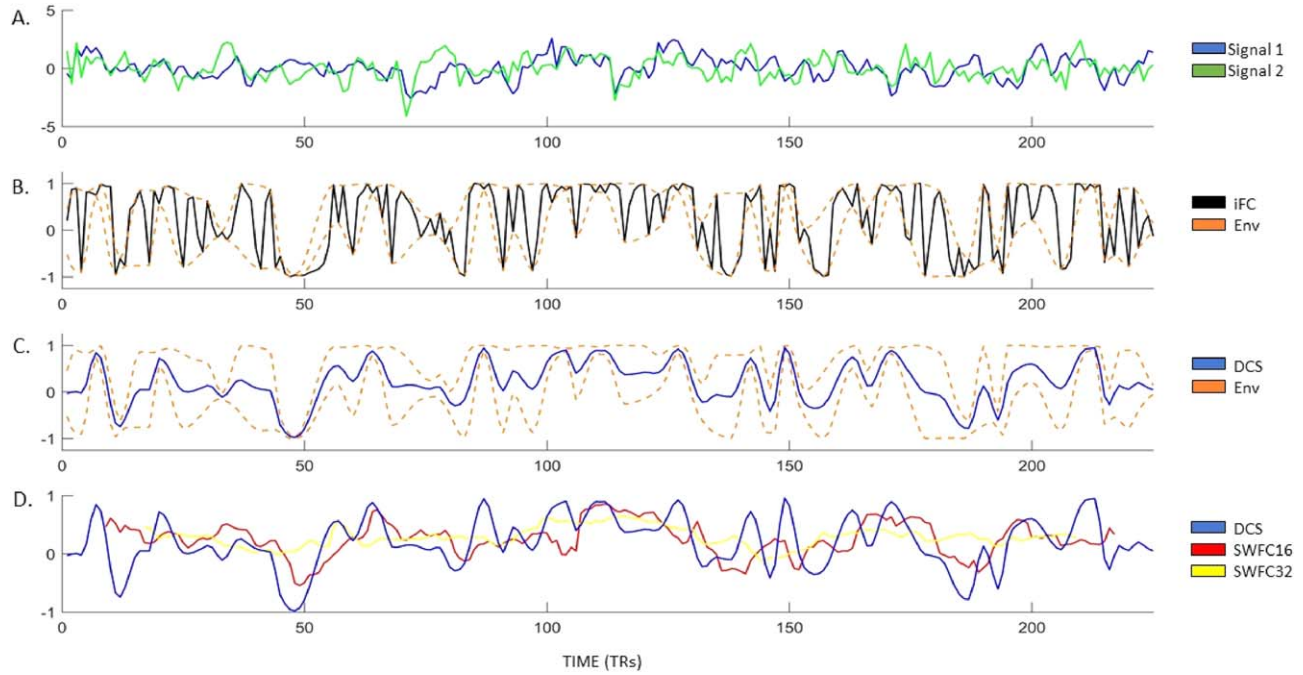

Figure 1.

The dynamic connectivity signal (DCS). Panel A: two regional fMRI brains signals (randomly chosen for illustration). Panel B: the instantaneous functional connectivity (iFC) is plotted in black. The upper and lower envelopes of the iFC are plotted as dashed orange lines. Panel C: the dynamic connectivity signal (DCS) is plotted in blue, along with the upper and lower envelope of the iFC as dashed orange lines. Panel D: the DCS is plotted in blue, along with sliding window functional connectivity (SWFC) for windows equal to 16 and 32 time points in red and yellow lines, respectively. Note that the SWFC time courses do not have measurements for all time points in the scan and that SWFC tends to smooth the time series over transient events identified by the DCS, but the major trends are conserved across all three metrics. [Color figure can be viewed at wileyonlinelibrary.com]

$200 \times 200 \times 16$ group DCS tensor, and decomposing it with parallel factor analysis (PARAFAC) [Carroll and Chang, 1970; Harshman, 1970].

PARAFAC with alternating least squares fitting was applied to the group DCS tensor to obtain a reduced-rank set of components that explain some portion of the data that is common across the group of participants. The PARAFAC model for a three-mode tensor is illustrated in Figure 3. The notation for the PARAFAC model given below, however, includes 4 modes because the symmetric DCS tensors constitute two spatial modes. PARAFAC decomposes the data into a sum of rank-one tensors (components) that approximates the data. Each rank-one tensor is the outer product of four vectors (factors),

$$X \approx \sum_{l=1}^{Rank} \lambda_l \; s_l \circ r_l \circ t_l \circ u_l, \tag{1}$$

wherefore X is the input tensor, $\circ$ denotes the vector outer product, and λ is the component weight. In Eq. 1, s corresponds to the time mode, r and t correspond to spatial modes (i.e., the pairwise connections of brain regions), and u corresponds to the participant mode that captures their individual variability. The optimization problem minimizes the difference between the data and its approximation at each iteration,

$$\text{Objective Function} \; -> \min \left\| X - \sum_{l=1}^{Rank} \lambda_l \; s_l \circ r_l \circ t_l \circ u_l \right\| \tag{2}$$

Each component (rank-one tensor) of the PARAFAC model represents a potential brain network, and includes four sets of factor loadings (s, r, t, and u from Eq. 1) corresponding to the four modes of the tensor. The vector s_l contains unit normalized factor loadings along the temporal mode that indicate synchronization strength of the component (network synchronization time course) at each time point. The spatial map is computed from factors in modes 2 and 3 as the outer product of two vectors, r_l and t_l from Eq. 1, which yields a 200×200 approximately symmetric matrix. The factor loadings in the spatial maps indicate the strength and direction of connections among regions. The factor loadings along the fourth mode, u, capture the individual variability of each participant (participant loadings) for each component. The factor loadings for each participant are scalar values that weight the remaining factors for that particular component. As such, the

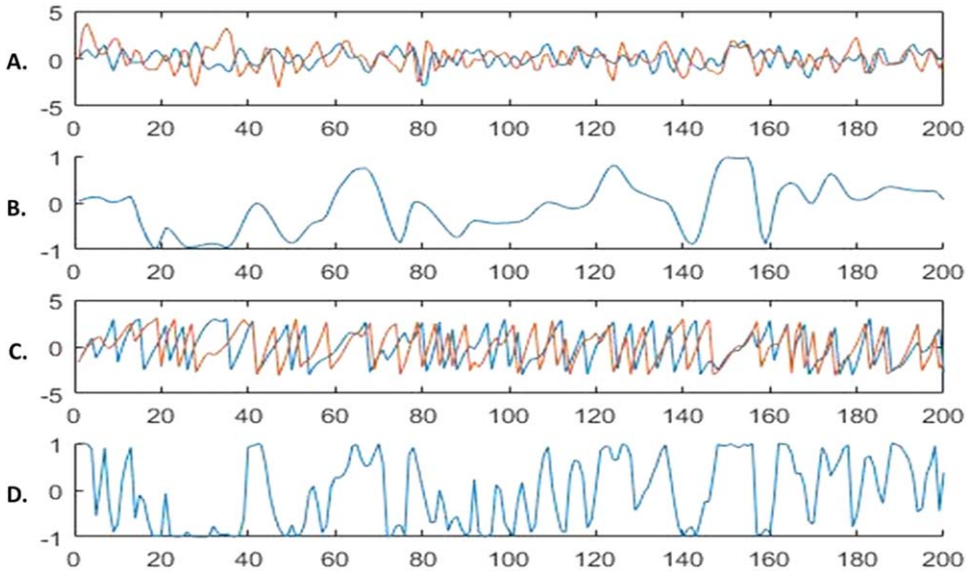

Figure 2.

The DCS and wideband signals. Panel A shows two random wideband signals. Panel B shows the DCS for the two signals. Panel C shows the phase vectors for the two signals. Panel D shows the iFC for the two signals. Visual inspection of Panel C reveals the characteristics of the DCS that make it suitable for wideband signals. The DCS indicates no synchronization from time points 1–15, where the phases are clearly not locked into the same frequency, but the iFC indicates rapidly fluctuating synchrony. Time points 20–30 show strongly antisynchronized signals (i.e., phases are 180° apart), and both the iFC and DCS are in agreement; however, at time point 40, the iFC indicates strong synchrony when in fact the phases are not locked onto the same frequency for the two signals; the DCS, in contrast, indicates no synchrony between the signals. Finally, time points 145–155 show that the phase vectors have locked onto the same frequency, and the signals are strongly synchronized; the iFC and DCS are in agreement. The DCS and iFC, however, fall out of agreement shortly after when the frequencies of the two signals again change at different rates; the iFC indicates rapidly fluctuating synchrony, whereas the DCS indicates no synchrony (see also time points 190–200). [Color figure can be viewed at wileyonlinelibrary.com]

participant factor indicates how strongly the data from that participant is represented in the other three modes of the tensor, namely, the time and spatial modes. A participant with a strong factor loading also strongly represents the temporal signature and spatial map, whereas a factor loading near zero would indicate that the participant's data does not contain a good match to the factor spatial map or time signature. This means that greater participant loadings in u_l indicate a stronger representation of the latent component in the data of that participant (the participant more strongly expressed the spatial map and time signature of the network identified by the component).

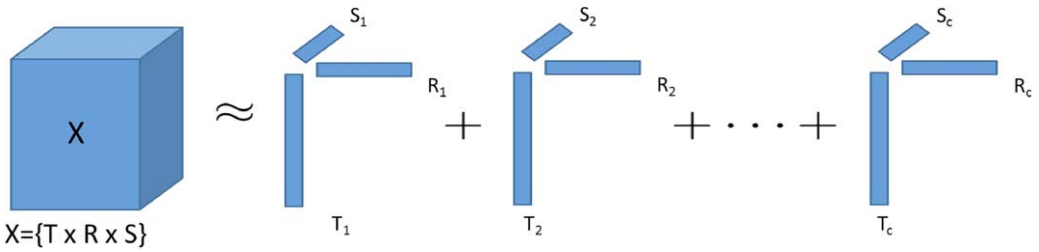

Figure 3.

Graphical depiction of the CANDECOMP/PARAFAC decomposition. The CANDECOMP/PARAFAC model decomposes a three-dimensional tensor, X, with dimensionality, *i, j, k*, into a sum of rank-one tensors, *l* (the number of components, or Rank). Each rank-one tensor is composed of a vector of latent factors along each mode, *r, s, t*, of the input tensor indicating the contribution of each variable to the component. [Color figure can be viewed at wileyonlinelibrary.com]

The PARAFAC decomposition was performed using the tensor toolbox version 2.6 [Bader and Kolda, 2015] and the number of components was set to 10 based on the aggregated estimated rank of each single subject dFC data set obtained from the core consistency diagnostic [Bro and Kiers, 2003; Papalexakis and Faloutsos, 2015]. The core consistency diagnostic indicates at what rank the core tensor of the PARAFAC solution satisfies the super-diagonal assumption of the PARAFAC model. The core consistency diagnostic has been demonstrated to work best among available techniques for estimating the rank of a PARAFAC tensor model [Morup and Hansen, 2009]. In addition, selection of 10 components is consistent with the rank selected by a previous study that used an alternative approach to estimate the optimal rank (i.e., DIFFIT) [Timmerman and Kiers, 2000] for a tensor factorization of resting state dFC [Ponce-Alvarez et al, 2015].

The PARAFAC decomposition is comparable to principal components analysis (PCA), but differs in that it operates on arrays with more than two modes (or dimensions) and does not impose constraints on spatial or temporal orthogonality. In the context of this application, the PARAFAC should perform better than models that impose orthogonality constraints if/when network configurations overlap spatially or have correlated time courses [Helwig and Hong, 2013]. The method of decomposing dFC is also comparable to the eigen connectivity method introduced by Leonardi et al. [2013], but does not require unfolding the tensor and collapsing two or more of the tensor modes. This allows for the investigation of individual variation in dFC through the analysis of the factor loadings in the participant mode (mode 4, u) of the PARAFAC model.

To identify the strongest connections within a network, brain networks derived from the matrix of spatial loadings were z-scored and thresholded at $\text{abs}(z) > 2.5$. This retains a maximum of 5% (995) of all possible connections (19,900) between regions. Two summary measures of brain regional connectivity were computed from the spatial maps. Network node degree was computed as the sum of binarized supra-threshold z-scored factor loadings for each region in the spatial maps, and network node strength was computed as the sum of the z-scored weights after thresholding. In addition, to define a statistical threshold for significant temporal factor loadings (i.e., time course of within network synchronization strength) we computed a 95% confidence interval by permuting the entire data set along the temporal and spatial modes and repeating the PARAFAC decomposition 1000 times.

Hypotheses and Planned Analyses

The main objective of this study was to identify whether individual differences in stressor-induced emotions are related to the transient synchronization dynamics of large-scale brain networks. We hypothesized that individual differences in subjective threat-related and stress relief-related positive and negative emotions would be reflected in the loadings of the participant mode for some factors, and, that some factor loadings from the temporal mode of the tensor would be correlated with the rest-task-recovery time structure of the SET, indicating their relevance for processing the task. In addition, we expected any emotion-related networks to be more strongly synchronized on average during the speech preparation and recovery periods than during the initial resting baseline period.

To test the first hypothesis, robust linear regression coefficients were computed between subjective emotion ratings and participant loadings of each factor. Outliers were identified as emotion ratings or factor loadings that were greater than 3 standard deviations from the group mean, and were removed prior to computing linear regression ($n = 1$). To investigate the second hypothesis, Pearson correlation coefficients were computed between each factor time course and a boxcar function (zeros and ones) corresponding to the rest-task-rest (recovery) design of the SET. The third hypothesis was tested with a series of two-sample t-tests on the average supra-threshold synchronization strength of relevant networks (identified from the outcome of analyses testing hypothesis 1) between the three main periods of the SET. For all regression, correlation and t-test analyses, we report P values that were corrected for multiple comparisons using the false discovery rate with $q = 0.05$ (FDR) [Benjamini and Hochberg, 1995], unless otherwise noted. Brain networks are visualized with the Brain Net Viewer (Xia, Wang & He, 2013).

In addition, because head motion during fMRI scanning can be a confounding source of variance in the recorded brain signals, which may subsequently confound correlations of functional connectivity with state and trait behavioral variables [Siegel et al, 2017], we conducted several ad hoc analyses of head motion to investigate its potential confounding effects for our hypothesis tests. The framewise displacement (FD), a measure of total head motion, was calculated for each participant. The average FD values from each participant were then used in zero-order correlation analyses to investigate whether the self-report emotion ratings were significantly related to head motion, essentially replicating the method employed by Siegel et al. [2017]. The average FD values were also examined in zero-order correlations with the participant loading vectors output by the PARAFAC. Also, the average FD was used as a covariate in the regression analyses to investigate whether head motion accounted for any findings relating emotion to brain networks identified by the PARAFAC decomposition (see next section for results). Additionally, we examined whether temporal fluctuations in FD was correlated with temporal fluctuations in network synchronization.

RESULTS

PARAFAC Four-Mode Components and Model Fit

Figure 4 shows each component of the PARAFAC tensor decomposition results. The PARAFAC model used in this

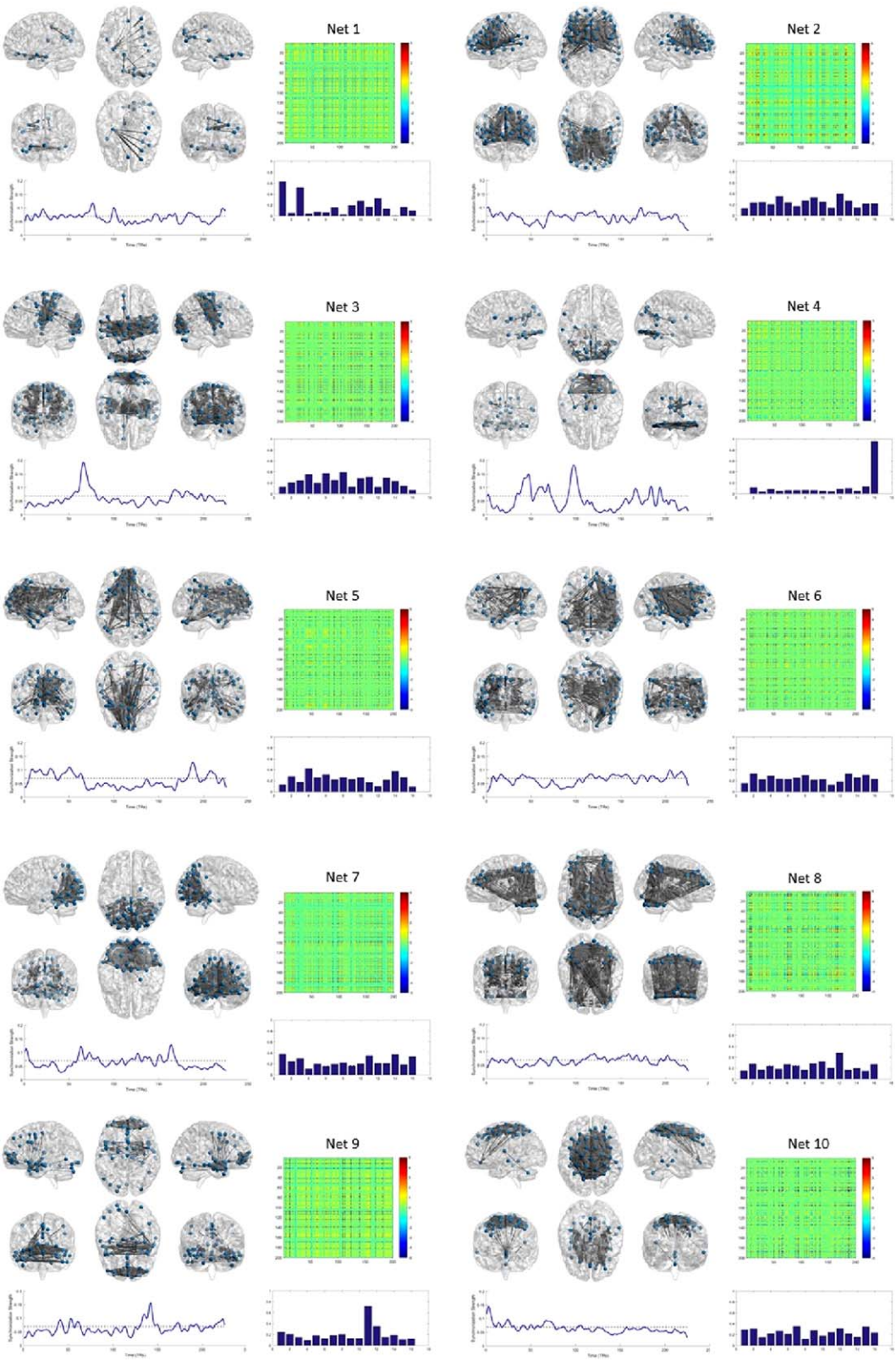

Figure 4.

The PARAFAC factors and brain network components. Each of the 10 components from the PARAFAC model are shown. Factor spatial loadings (i.e., networks) are shown in matrix form unthresholded. Brain maps are thresholded at abs(z) $>$ 2.5. Participant loading vectors are shown as bar graphs. The time course from each component has network synchronization strength (the time course of factor loadings) plotted on the *y*-axis and time on the *x*-axis. [Color figure can be viewed at wileyonlinelibrary.com]

study did not impose constraints for non-negativity, yet all participant loadings and temporal loadings were unanimously non-negative. Also, the model did not include symmetry constraints for the two spatial modes, but it produced spatial factors that were approximately symmetric. Each of the components from the PARAFAC model represents a network of brain regions whose pairwise synchrony fluctuated in a coordinated manner, either driven by the task or other internal regulating factors. The synchronization threshold based on the empirically derived distribution of permuted replicates was 0.063 (threshold based on 95% confidence interval that ranged from 0.0605 to 0.0651). Values that exceed this interval indicate statistically significant synchronization of a brain network at a given time point.

Correlations of Participant Factor Loadings and Individual Differences in Subjective Emotions

To test the main hypothesis that individual differences in emotions is related to individual differences in dFC, we calculated the correlation between the self-report emotion ratings and the participant loadings for each PRAFAC component. The regression model included emotion ratings and FD as the two predictor variables (FD was a covariate of no interest; see also analyses of head motion confounds in the section below), and factor loadings as the dependent variable. There were no significant correlations among the participant factor loadings and the retrospective ratings of relief-related positive or negative emotion. The participant factor loadings for two networks were significantly correlated with the threat-related positive and negative emotions, as shown in Figure 5. The participant loadings for network 8 were positively correlated with negative emotion, beta = 0.041, $t(15) = 3.58$, $P = 0.0037$ (FDR-adjusted $P = 0.038$), and the participant loadings from network 9 were positively correlated with positive emotion, beta = 0.0384, $t(15) = 3.73$, $P = 0.0029$ (FDR-adjusted $P = 0.029$).

Figure 5 panels A and B show the network connectivity (correlated and anticorrelated), and the MNI coordinates of the top 10 most interconnected brain regions are listed in Tables I and II, along with values for node degree and node strength. For the network related to negative emotions (comp8), brain regions with the highest node degree included the right midcingulate, parietal cortex, cerebellum and right middle frontal gyrus (correlated synchronization), and the right insula and superior temporal gyrus (anticorrelated synchronization). It did not include functional connectivity with the vmPFC. For the network related to positive emotions (comp9), brain regions with the highest node degree included the vmPFC (listed as frontal medial orbital in the Table II), middle temporal gyrus and ACC (correlated synchronization), and right superior frontal gyrus, inferior frontal gyrus and ACC (anticorrelated synchronization). The regions with significant connections to the vmPFC for the positive emotion network are listed in Table III.

The amygdala was significantly involved in both the positive and negative emotion networks, its role being primarily anticorrelated with small clusters of scattered brain regions (Fig. 6A). Tables IV and V report the regions that showed significant connectivity with the amygdala for these two emotion-related networks. In the positive emotion network, the left and right amygdala showed mostly significant anticorrelations with regions of the vmPFC, and a few positively weighted connections with the right anterior temporal lobe (Table IV). In the negative emotion network, the left amygdala (but not the right) showed negatively weighted connectivity with the cerebellum, ACC, and posterior regions in the parietal cortex (Table V).

Figure 6B and C depicts the significant connectivity for the anterior insula and cingulate cortex for both the negative and positive emotion networks. A full list of significant connections for these regions appears in Supporting Information, Tables S1–S4. The right and left insula together had the most significant anticorrelated connections within the negative emotion network, with 57 significant anticorrelated connections in total. Among the strongest anticorrelated insula connections were the left and right inferior parietal cortex, left cerebellum, right middle frontal gyrus, right precueneus, and the left and right midcingulate gyrus. There was only one significant positive connection, which occurred between the left and right insula (interhemispheric synchrony for the anterior insula). For the positive emotion network, there were five positive connections from the insula bilaterally to the right anterior temporal cortex (temporal pole and middle temporal gyrus). There were strong anticorrelations with the anterior ventral PFC (Fig. 6B), and the ACC.

The cingulate gyrus was also involved in both emotion-related networks (Fig. 6C). Whereas the positive emotion network involved significant connectivity of the ACC and midcingulate, the negative emotion network involved connectivity of the mid- and posterior cingulate cortex. For the positive network, the cingulate cortex was often anticorrelated between the hemispheres (Supporting Information, Table S3), and also included anticorrelations with the insula and amygdala. For the negative emotion network, the right midcingulate had 21 of the 22 strongest connection weights among the cingulate regions (extending from anterior to posterior). Some of the connected regions include bilateral connectivity between the left and right midcingulate regions, left cerebellum, right inferior parietal cortex, right middle frontal gyrus, and right precuneus. It also included anticorrelated connections with the left and right insula, lingual gyrus, calcarine gyrus, and amygdala (see Supporting Information, Table S4 for a complete list).

Temporal Correlations Among Networks and the SET

To test the second hypothesis that the time signature of some networks is associated with the task design, we

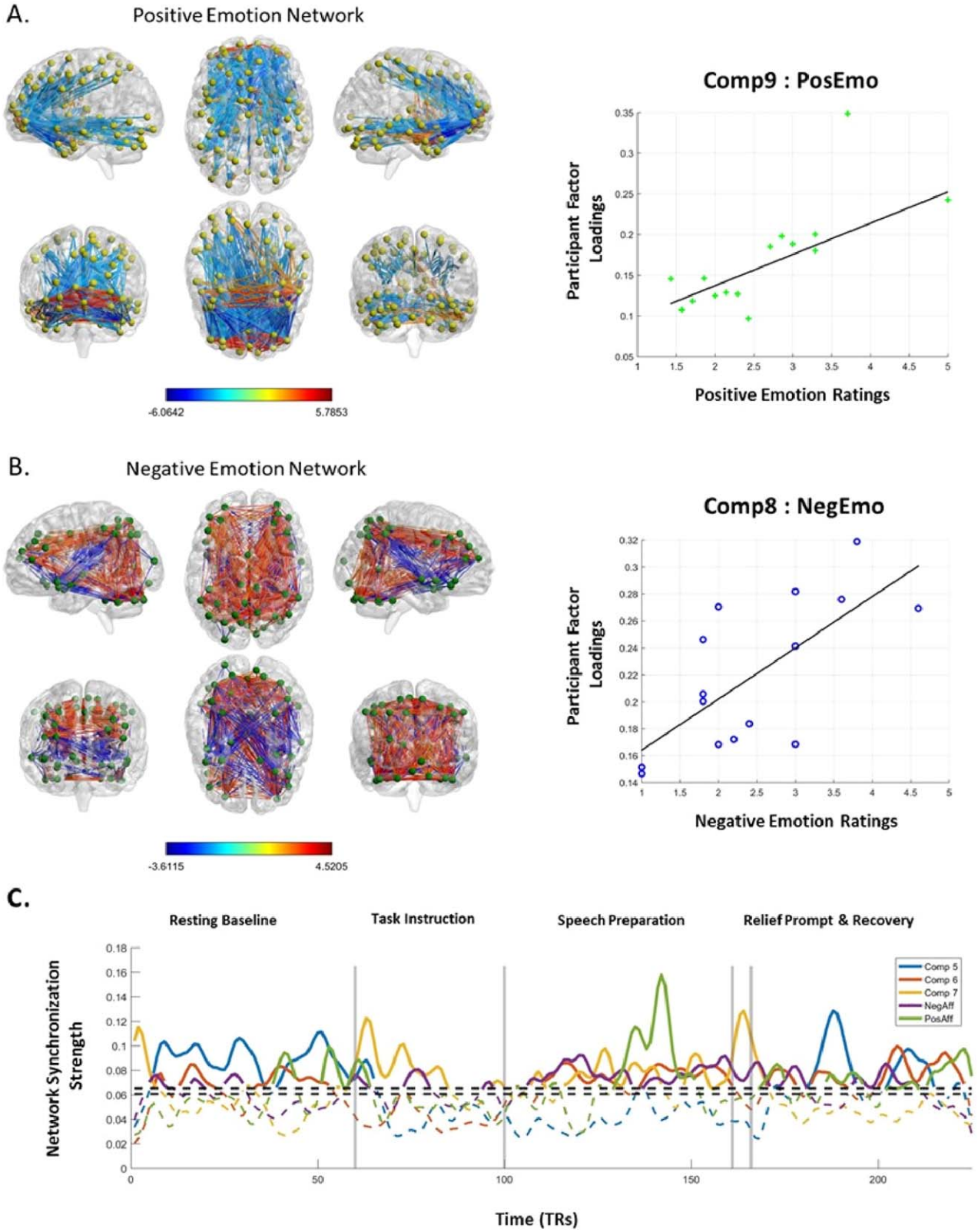

Figure 5.

Networks for positive and negative emotions. Panel A shows the positive and negative spatial factor loadings for the positive emotion network, and the scatterplot and best fit regression line between subjective positive emotion ratings and factor loadings. Panel B shows the positive and negative spatial factor loadings for the negative emotion network, and the scatterplot and best fit regression line between subjective positive emotion ratings and factor loadings. Panel C shows the time signatures for the 5 SET relevant network components. The dashed horizontal line indicates the empirically derived statistical threshold of temporal factor loadings and serves to illustrate that the time signatures of the 5 relevant networks fluctuate throughout the task. [Color figure can be viewed at wileyonlinelibrary.com]

TABLE I. Negative emotion network

MNI *x*, *y*, *z* coordinates					
x	*y*	*z*	Anat. label	Node degree (°)	Node strength
9.1	−35.9	47.1	Cingulum_Mid_R	39	138.03
55.2	−47.5	41.9	Parietal_Inf_R	38	132.48
−40.1	−52.6	−33.2	Cerebelum_Crus1_L	38	129.80
31.7	54.8	14.9	Frontal_Mid_R	38	126.62
−36.7	−71	−31.6	Cerebelum_Crus1_L	38	137.43
40.6	−43.2	48.2	Parietal_Inf_R	38	125.61
−33.9	−53.8	49.5	Parietal_Inf_L	38	136.42
32.9	44.6	28.1	Frontal_Mid_R	38	126.89
1.6	−16.5	34.8	Cingulum_Mid_R	37	121.90
10.3	−63.5	56.2	Precuneus_R	37	122.57
47.8	7.9	−9.3	Insula_R	30	−92.23
−28.9	12.1	−16.6	Insula_L	27	−78.11
58.4	−7.8	−7.8	Temporal_Sup_R	27	−77.89
−11.3	−70.4	5.9	Calcarine_L	24	−66.57
18.2	−55.5	3.2	Lingual_R	24	−67.45
−46.4	13.8	−11.2	Temporal_Pole_Sup_L	23	−64.90
−45	−0.7	−14.6	Temporal_Sup_L	18	−49.63
29.6	24.6	−15.1	Frontal_Inf_Orb_R	15	−41.08
−36.7	−71	−31.6	Cerebelum_Crus1_L	15	−44.69
−13.3	−52.9	−0.7	Lingual_L	15	−40.44

calculated the correlations between the time loadings of each PARAFAC component and a boxcar function representing the SET task. The time courses of factor loadings for network 5 and 6 were significantly anticorrelated to the rest-task-recovery task design, rs = −0.66 and −0.23, with Ps < 0.05 (FDR corrected), respectively. Networks 7 and 8 (the negative emotion network) were significantly positively correlated to the task design, rs = 0.46 and 0.32, with Ps < 0.05 (FDR corrected). The time course for network 7 was most strongly positively correlated with the task design, and included prominent peaks at the onset of visual stimulation signaling the start and end of the task and mostly involved the occipital cortex suggesting it reflects a vision network. No other network time courses

TABLE II. Positive emotion network

MNI *x*, *y*, *z* coordinates					
x	*y*	*z*	Anat. label	Node degree (°)	Node strength
55.1	−3.6	−25.4	Temporal_Mid_R	38	114.88
45.7	13.3	−22.7	Temporal_Pole_Sup_R	24	71.32
−40.6	12.9	−28.2	Temporal_Pole_Mid_L	12	36.58
27.7	58.2	−1.6	Frontal_Sup_R	11	50.77
6.7	42.6	6.1	Cingulum_Ant_R	11	45.30
1.4	55.9	−7.2	Frontal_Med_Orb_R	11	49.05
28.3	43.8	−13.5	Frontal_Mid_Orb_R	11	44.65
−6.8	45.7	7.8	Cingulum_Ant_L	10	36.94
−28.3	50.7	−11.6	Frontal_Mid_Orb_L	10	38.22
−0.1	38.9	−12.2	Frontal_Med_Orb_L	10	31.08
27.7	58.2	−1.6	Frontal_Sup_R	81	−271.68
1.4	55.9	−7.2	Frontal_Med_Orb_R	75	−249.97
6.7	42.6	6.1	Cingulum_Ant_R	63	−201.13
28.3	43.8	−13.5	Frontal_Mid_Orb_R	58	−187.72
42.9	49.6	−4.4	Frontal_Mid_Orb_R	56	−181.49
−40.9	48.7	−3.4	Frontal_Mid_Orb_L	50	−152.85
−28.3	50.7	−11.6	Frontal_Mid_Orb_L	49	−148.28
10.7	63	10	Frontal_Sup_Medial_R	47	−141.49
−6.8	45.7	7.8	Cingulum_Ant_L	46	−136.12
−27.8	56.9	4.7	Frontal_Mid_L	28	−84.01

TABLE III. vmPFC connectivity for positive emotion network

Anat. label	*x*	*y*	*z*	Edge loading
Left vmPFC (−0.1 38.9 − 12.2)				
Frontal_Med_Orb_R	1.4	55.9	−7.2	7.2002934
Frontal_Sup_R	27.7	58.2	−1.6	3.7554923
Cingulum_Ant_R	6.7	42.6	6.1	3.2980712
Frontal_Mid_Orb_R	28.3	43.8	−13.5	3.2444432
Frontal_Mid_Orb_R	42.9	49.6	−4.4	3.2170145
Frontal_Mid_Orb_L	−40.9	48.7	−3.4	2.9084984
Frontal_Mid_Orb_L	−28.3	50.7	−11.6	2.8995669
Frontal_Sup_Medial_R	10.7	63	10	2.8246006
Cingulum_Ant_L	−6.8	45.7	7.8	2.7955437
Frontal_Mid_L	−27.8	56.9	4.7	2.5379621
Right vmPFC (1.4 55.9 − 7.2)				
Frontal_Med_Orb_L	−0.1	38.9	−12.2	7.2002934
Frontal_Sup_R	27.7	58.2	−1.6	5.7853042
Cingulum_Ant_R	6.7	42.6	6.1	5.0981223
Frontal_Mid_Orb_R	28.3	43.8	−13.5	5.0329169
Frontal_Mid_Orb_R	42.9	49.6	−4.4	4.9915915
Frontal_Mid_Orb_L	−40.9	48.7	−3.4	4.5267667
Frontal_Mid_Orb_L	−28.3	50.7	−11.6	4.4994509
Frontal_Sup_Medial_R	10.7	63	10	4.4003623
Cingulum_Ant_L	−6.8	45.7	7.8	4.3431774
Frontal_Mid_L	−27.8	56.9	4.7	3.9684993
Olfactory_R	0.1	20.4	−8	2.8065213

showed a significant correlation or anticorrelation with the task design that survived the FDR correction. The most strongly connected regions (positive and negative) of the network identified by component 6, which had a task-relevant network time signature, are listed in Table VI.

The time courses from the 10 networks are not constrained to be temporally orthogonal by the PARAFAC model and showed a variety of inter-correlations (Table VII). Most notably, the time courses for the networks associated with positive and negative emotions were not significantly correlated, $P > 0.05$, indicating that they fluctuate in synchronization strength independently of each other. As one might expect, the time course of component 5, which was anticorrelated with the task structure, was also anti-correlated with the time course of components that were positively correlated to the task structure (comp7 [visual network] and comp8 [negative emotion network]). The time course of factor loadings for the positive emotion-related network (comp9) was significantly correlated only with the time course of comp6 (which also had a task-relevant time signature), but was uncorrelated with all other networks and the rest-task-rest SET task structure.

Task-Related Dynamics of Emotion-Related Networks

The average synchronization strength of the time course for the networks correlated with positive and negative emotions was compared among the 3 main SET task periods (resting baseline, task, recovery). For each time course, time points below the empirically derived statistical threshold for significant synchronization were set to 0, and a two-sample t-test was performed on the synchronization values from each period to test whether the average supra-threshold synchronization strength of either network varied as a function of SET task period. The synchronization strength of the positive emotion network seemed to grow from baseline to the task period, $t(152) = -1.89$, $P = 0.06$ (uncorrected), and from the task period to recovery, $t(163) = -2.48$, $P = 0.014$ (uncorrected). The synchronization strength was also significantly stronger during recovery than the initial resting baseline, $t(112) = -4.75$, $P = 0.0000006$ (uncorrected). On the other hand, the synchronization strength of the negative emotion network was most prominent during the task period, which was significantly stronger than during both the baseline, $t(121) = 5.21$, $P = 0.0000007$ (uncorrected), and recovery periods, $t(107) = 2.56$, $P = 0.012$ (uncorrected). Notably, the synchronization strength of the negative emotion network was also stronger during recovery than during the resting baseline, $t(112) = -2.10$, $P = 0.037$ (uncorrected). These results show that the positive and negative emotion networks were more active during the speech preparation period than during the resting baseline, and that synchronization of the positive emotion network resurged during the recovery period.

Correlations of Head Motion with Emotion Ratings and Factor Loadings

Head motion was, inevitably, present in all participants' data. One participant had substantially greater FD (.99 mm) than the other participants (approximately 3 standard deviations greater); however, this participant was not excluded because this amount of head movement is considerably less than the size of a voxel (3.5 mm^3) collected in this study. This indicates that there was a relatively small amount of head movement in the sample of participants.

The average FD of each participant was not significantly correlated with the four ratings of emotions (positive stressor $r = -0.23$, $P = 0.39$; positive relief $r = 0.20$, $P = 0.45$, negative stressor $r = -0.21$, $P = 0.42$, negative relief $r = -0.23$, $P = 0.38$). The group average (s.d.) FD during each of the scanning periods was 0.20 (.32), 0.27 (.39), 0.12 (.08), 0.33 (.53), and 0.20 (.15) mm. None of these were significantly different using two-sample t-tests with all Ps > 0.05. Furthermore, these epoched FD values from each participant were not significantly correlated with any of the emotion ratings with all Ps > 0.05.

There was a strong zero-order correlation of head motion with participant loadings of component 4, $r = 0.91$, $P = 0.0000013$, and it can be seen that the participant with the greatest FD (participant 16) dominated this factor with

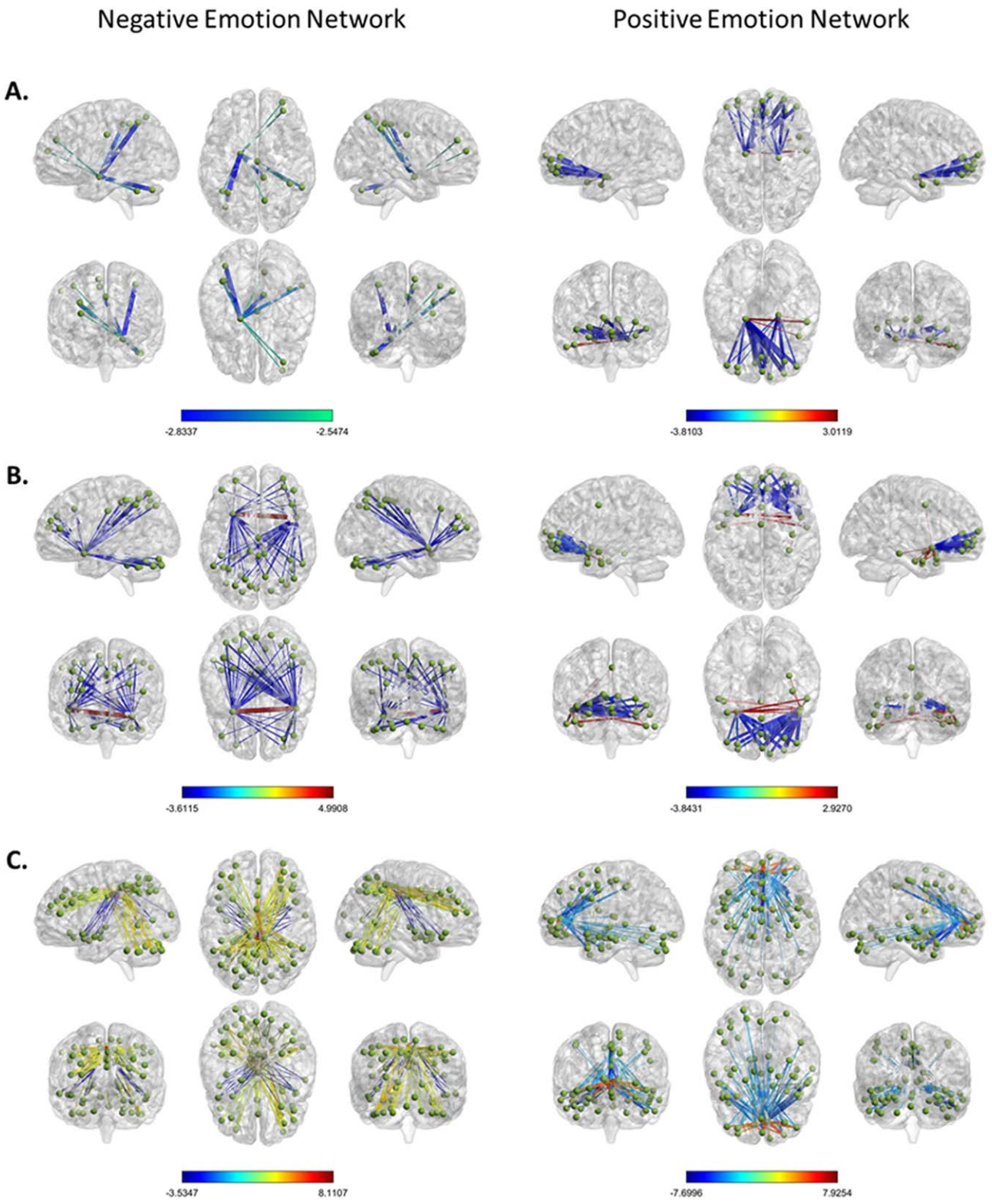

Figure 6.

Amygdala, insula, and ACC connectivity for negative and positive emotion networks. Panel A shows significant amygdala connectivity for the negative emotion network (left) and positive emotion network (right). Panel B shows significant connectivity for the anterior insula for the negative emotion network (left) and positive emotion network (right). Panel C shows significant connectivity for the cingulate cortex for the negative emotion network (left) and positive emotion network (right). [Color figure can be viewed at wileyonlinelibrary.com]

TABLE IV. Amygdala connectivity for positive emotion network

Anat. label	*x*	*y*	*z*	Edge loading
Left amygdala (−18.7 − 7.4 −15.9)				
Temporal_Mid_R	55.1	−3.6	−25.4	3.011853
Temporal_Pole_Sup_R	45.7	13.3	−22.7	2.720626
Frontal_Med_Orb_L	−0.1	38.9	−12.2	−2.54163
Frontal_Mid_L	−27.8	56.9	4.7	−2.80282
Cingulum_Ant_L	−6.8	45.7	7.8	−2.97303
Frontal_Sup_Medial_R	10.7	63	10	−3.05837
Frontal_Mid_Orb_L	−28.3	50.7	−11.6	−3.06376
Frontal_Mid_Orb_L	−40.9	48.7	−3.4	−3.13317
Frontal_Mid_Orb_R	42.9	49.6	−4.4	−3.40822
Cingulum_Ant_R	6.7	42.6	6.1	−3.41135
Frontal_Mid_Orb_R	28.3	43.8	−13.5	−3.43267
Frontal_Med_Orb_R	1.4	55.9	−7.2	−3.74979
Frontal_Sup_R	27.7	58.2	−1.6	−3.81033
Right amygdala (21.3 − 11.9 − 16.4)				
Temporal_Mid_R	55.1	−3.6	−25.4	2.563685
Cingulum_Ant_L	−6.8	45.7	7.8	−2.61848
Frontal_Sup_Medial_R	10.7	63	10	−2.64136
Frontal_Mid_Orb_L	−28.3	50.7	−11.6	−2.69724
Frontal_Mid_Orb_L	−40.9	48.7	−3.4	−2.76877
Frontal_Mid_Orb_R	42.9	49.6	−4.4	−2.93869
Frontal_Mid_Orb_R	28.3	43.8	−13.5	−2.94968
Cingulum_Ant_R	6.7	42.6	6.1	−2.99898
Frontal_Med_Orb_R	1.4	55.9	−7.2	−3.23622
Frontal_Sup_R	27.7	58.2	−1.6	−3.34532

a loading that was much greater (∼3 standard deviations) than all other participants. As such, this component is considered a noise component of no interest. None of the remaining components had a significant zero-order correlation with participants' head motion. The zero-order correlations for the 5 components of interest (identified in the results reported above) were non-significant (comp5 $r = -0.58$, $P = 0.09$, comp6 $r = -0.15$, $P = 0.93$, comp7 $r = 0.37$, $P = 0.40$, comp8 $r = 0.04$, $P = 0.97$, and comp9 $r = -0.13$, $P = 0.93$).

We also examined whether temporal fluctuations in head movement was correlated with temporal fluctuations in network synchronization identified by the PARAFAC decomposition by using the temporal FD as predictor variables in a series of group linear regression models with network synchrony as dependent variable. The time course of FD for each participant was significantly correlated with the time courses of components 3 and 4, betas = −0.13 and 0.09, ts(15) = 2.45 and 3.40, Ps = .003 and .0004. Component 4 was already identified as a noise component, and component 3 can also be considered a noise component as well. No other component time courses were correlated with head motion. Taken together, these results indicate that emotion ratings were neither related to movement in the scanner throughout the experiment, nor during any specific time or task period, and that only 2 of the 10 components were confounded by noise from head motion, although they were unrelated to emotion ratings and the SET task.

DISCUSSION

The aim of this study was to identify whether individual differences in subjective emotions in response to acute psychosocial stress are reflected in the synchronization dynamics of large-scale brain networks. Results of this study indicate that individual differences in positive and negative emotions were significantly correlated with individual differences in the synchronization strength for two large-scale brain networks that involved the vmPFC, amygdala, anterior insula, and ACC. The time-courses of the emotion networks were not significantly correlated with each other, and were more strongly synchronized (within network) during the speech preparation and recovery periods than during the initial resting baseline period. Furthermore, several ad hoc analyses of head movement using the method of Siegel et al. [2017] indicate that relations between the psychological variables and brain networks were not directly attributable to motion related confounds. In sum, these findings indicate that individual differences in stress-induced emotional intensity are reflected in the synchronization dynamics of large-scale brain networks involving the vmPFC, amygdala, ACC, and insula, and that the synchronization strength of these emotion-related networks resurges during poststressor recovery.

Individual Differences in Emotion

The network correlated with individual differences in subjective negative emotional intensity comprised long-distance synchronization among lateral PFC, posterior parietal cortex, and the cerebellum. It did not include connectivity with the vmPFC, but did include negative functional connectivity with both the anterior insula and

TABLE V. Amygdala connectivity for negative emotion network

Left amygdala (−18.7 − 7.4 −15.9)				
Anat. Label	*x*	*y*	*z*	Edge loading
Cingulum_Mid_R	1.6	−16.5	34.8	−2.54737
Precuneus_R	10.3	−63.5	56.2	−2.59356
Frontal_Mid_R	31.7	54.8	14.9	−2.60356
Parietal_Inf_R	40.6	−43.2	48.2	−2.60719
Frontal_Mid_R	32.9	44.6	28.1	−2.63509
Cerebelum_Crus1_L	−40.1	−52.6	−33.2	−2.65708
Parietal_Inf_R	55.2	−47.5	41.9	−2.71353
Cingulum_Mid_R	9.1	−35.9	47.1	−2.77584
Cerebelum_Crus1_L	−36.7	−71	−31.6	−2.80727
Parietal_Inf_L	−33.9	−53.8	49.5	−2.83371

TABLE VI. Highly connected regions for component 6

MNI *x*, *y*, *z* coordinates			Anat. label	Node degree	Node strength
x	*y*	*z*			
55.2	−47.5	41.9	Parietal_Inf_R	35	120.35
61.9	−21.1	−15.6	Temporal_Mid_R	34	113.89
44.9	−65.5	39.3	Angular_R	34	115.37
55.1	−28.8	0.1	Temporal_Sup_R	32	103.89
42.4	23.8	37.6	Frontal_Mid_R	24	78.15
−51.9	−50.2	42.1	Parietal_Inf_L	24	78.36
55.1	−3.6	−25.4	Temporal_Mid_R	24	78.22
−58.9	−30.2	−2.4	Temporal_Mid_L	22	67.67
53.8	−55.4	23.5	Angular_R	22	67.81
−56.4	−15.1	−15.3	Temporal_Mid_L	22	68.27
22.5	−69.6	−11.3	Lingual_R	27	−87.92
55.2	−47.5	41.9	Parietal_Inf_R	21	−66.03
44.9	−65.5	39.3	Angular_R	21	−64.61
61.9	−21.1	−15.6	Temporal_Mid_R	20	−61.15
8.1	−74	6.5	Calcarine_R	20	−61.45
55.1	−28.8	0.1	Temporal_Sup_R	19	−56.08
−5.4	−87.2	25	Cuneus_L	18	−52.13
−14.3	−74.2	−10.1	Lingual_L	18	−53.05
−11.3	−70.4	5.9	Calcarine_L	17	−48.85
18.2	−55.5	3.2	Lingual_R	15	−42.68

amygdala. The topography of this negative emotion network strongly resembles the previously reported 'task positive' network [Fox et al., 2005]. The task positive network is composed of fronto-parietal regions that are co-activated and synchronized when engaged with an exogenous sensory-motor task. Previous research has shown that autonomic components of stress-related arousal, such as skin conductance levels (SCL) and heart rate (HR), are differentially related to a similar network topography involving the fronto-parietal cerebellar network [Eisenbarth et al, 2016], suggesting that SET task engagement is associated with autonomic components of stress and emotion, which may in turn cause the relationship with negative emotions. Furthermore, it is possible that those participants who experienced greater negative emotion in anticipation of the psychosocial stressor (i.e., evaluation of the speech) more strongly engaged the task positive network for speech preparation (i.e., exerted more effort for preparing the speech), which may indicate that stronger negative emotions motivated more vigorous preparation to reduce the perceived threat. Indeed, motivational factors can alter the autonomic and neural underpinnings of anticipatory social evaluative threat [Smith et al., 1997].

The spatial topography of brain regions comprising the positive emotion network is consistent with previous reports of the anterior vmPFC being involved in the processing of positive emotions and resilience to stress [van der Werff et al., 2013; Urry et al, 2006; Motzkin et al., 2015; Ong et al., 2006], and affective self-regulation [Motzkin et al, 2014], and the subjective decision to downregulate negative emotion [Dore et al., 2017]. This network was composed of dense connectivity among ventral PFC regions and the PFC connectivity was interhemispheric, involving both lateral and medial ventral regions. It also included connectivity with the right and left ACC, and negative functional connectivity with the amygdala and anterior insula, which is consistent with its function of down-regulating conscious negative emotions, either via appraisal/reappraisal, or some other mechanism.

Temporal Dynamics of Emotion-Related Networks

The temporal dynamics of the two emotion-related brain networks were temporally independent from each other. That the two emotion-related networks are neurodynamically independent, and not anticorrelated, is an important finding because it demonstrates that networks for positive and negative emotions are not strictly opponent processes. This is consistent with the notion that positive and negative emotions may make simultaneously unique contributions to stress and coping [Folkman, 2008], and implies that concurrent synchronization of these two networks, and their transient interactions, may underpin complex mixed emotions [Rafaeli et al., 2007].

Poststress resting-state functional connectivity among the amygdala and numerous cortical regions is reportedly altered after exposure to a psychosocial stressor [van

TABLE VII. Network time course intercorrelations

	Comp2	Comp3	Comp4	Comp5	Comp6	Comp7	Comp8	Comp9	Comp10
Comp1	−0.199*	0.239**	0.178*	0.087	−0.187*	0.039	−0.359***	−0.017	0.184*
Comp2	−	−0.102	−0.180*	−0.145	0.001	0.048	0.204**	−0.324***	0.274***
Comp3	−	−	0.341***	−0.0384	−0.332***	0.284***	−0.075	−0.016	0.132
Comp4	-	-	-	0.024	−0.273***	−0.049	−0.267***	−0.214**	0.111
Comp5	-	-	-	-	0.189*	−0.455***	−0.358***	0.070	0.059
Comp6	-	-	-	-	-	−0.395***	0.180*	0.345***	−0.434***
Comp7	-	-	-	-	-	-	0.326*	−0.106	0.281*
Comp8	-	-	-	-	-	-	-	−0.094	−0.117
Comp9	-	-	-	-	-	-	-	-	−0.432***

*$P < 0.05$, **$P < 0.005$, *** $P < 0.001$ (P values FDR corrected).

Marle et al., 2010; Veer et al., 2012; Vaisvaser et al, 2013], and poststressor resting state FC between the amygdala and the perigenual ACC is correlated with stressor-induced blood pressure reactivity [Gianaros et al., 2008]. Together, these resting state FC studies show that brain networks associated with stressor-induced negative emotions and physiology may either persist or resurge during post-stressor recovery.

Our findings suggest that within network synchrony of both the positive and negative emotion networks is resurgent after relief from the stressor, rather than persisting from their initial synchronization. The neurodynamics of the positive emotion network demonstrated interesting behavior in that it was not significantly correlated with the SET task structure, but it showed strong synchrony late in the stressor period before the onset of the relief and recovery period. This suggests that this positive emotion network is not necessarily tied to speech preparation but rather to spontaneous processes that occurred toward the end of speech preparation and after participants were told that they would not have to give a speech. For example, the healthy participants in this study may have experienced a positively valenced reappraisal of the stressor after engaging in speech preparation, or they may have experienced internally generated relief after having covertly prepared an adequate speech that may avert the looming evaluative threat. Moreover, connectivity within this network demonstrated resurgent synchrony during the recovery period (especially later in the recovery period – the green signal in Fig. 4C). This further suggests that some emotion-related neural signals that appear during stress may subsequently alter the course of the stress response, exacerbating or mitigating it, by reactivating various emotional memories after disengagement from the stressor. These formulations are highly speculative, however, and will need to be tested in future investigations.

The Amygdala and Emotion-Related SET Networks

Functional connectivity with the amygdala for both the emotion-related networks was primarily anticorrelated. This is consistent with previous research that has reported amygdala deactivation during engagement with the SET, in combination with activation of the ventral PFC and task performance networks [Wager et al, 2009a, 2009b]. While participants indeed experience negative emotions because of the SET, it is puzzling why the amygdala is not directly involved. There are several possible reasons why the amygdala may be deactivated during the speech preparation period of the SET. One reason is that it serves as an automatic prophylactic response against the anticipated forthcoming negative evaluations. Another reason is that the amygdala is primarily involved in predictive cues for threat, rather than conscious experience of the stressor per se, as advocated by Wager et al. [2009a]. Either of these hypotheses could be tested in future studies. For example, investigating whether the magnitude of amygdala deactivation is dependent on the intensity of the perceived threat could test the first hypothesis, and an experiment that compares amygdala deactivation during the presentation of a conditioned stimulus that signals social threat versus engaging the social stressor as an unconditioned stimulus could address the second hypothesis.

Importantly, the positive and negative emotion networks overlapped in their negative functional connectivity with the amygdala, but there were no regions of overlap between the positive and negative emotion networks via the amygdala (no regions in common that showed connectivity with the amygdala), and their respective time courses were not correlated. Moreover, it indicates that the activity of the vmPFC of the positive emotion network, and several key regions of the negative emotion network (ACC, cerebellum, parietal cortex), respond to the stressor differently from each other and yet both are anticorrelated with the amygdala. Together, these suggest that the amygdala plays two separate roles during the SET. It is possible that the amygdala integrates information between these two networks, or that it regulates switching between a large-scale brain topography that is relatively dominated by the synchrony of either one of the two networks.

The Insula and Cingulate Cortex

The anterior insula and ACC are core regions of the salience network [Seeley et al, 2007]. The salience network is related to trait anxiety and is involved in detecting important environmental events and signaling switches between task-engaged and default connectivity profiles. The salience network, as described by Seeley and colleagues, appears not to be a coherent part of the emotion-related networks detected in this study despite involving connectivity with the anterior insula and ACC. The positive emotion network involved connectivity among the ACC and the vmPFC, and anticorrelated connectivity with the insula, indicating a fractionation of the salience network. The negative emotion network seems to be a task positive network, which is a separate network altogether from the salience network, again despite including some connectivity with the insula and cingulate cortex. Connectivity of regions involved in the negative emotion network with the insula was anticorrelated, and while the cingulate cortex was involved in this network, it was more posterior than regions typically involved in the salience network. As such, it appears that the anterior insula, and multiple regions of the cingulate gyrus, extending from anterior to posterior, are performing functions that are distinct from those related to the salience network reported by Seeley and colleagues.

Previous research concerning psychosocial stress has implicated the insula in several processes, including interoceptive awareness of autonomic arousal in relation to

conscious emotional experience [Terasawa et al., 2013], and psychological resilience to negative events [Waugh et al, 2008]. Given their parallel functional connectivity in the positive and negative emotion-related brain networks in this study, similar to the amygdala, it is possible that these regions are performing integrative functions, leading to a higher order brain control (i.e., network-based rather than region-based) over autonomic arousal, and downregulating interoceptive awareness of autonomic indicators of the social threat to better prepare a response and suppress the threat altogether. While this explanation is speculative, it can be tested empirically by examining the correlation among perceived threat, interoceptive awareness of autonomic arousal related to the threat, and speech performance and autonomic responding to negative social feedback about the speech performance.

Physiological Arousal and Dynamic Functional Connectivity

We did not measure autonomic physiological signals throughout the stressor, but this is not simply a limitation of the study. Physiological processes, such as respiration and cardiac cycles, significantly modulate spontaneous dFC [Nikolau et al., 2016], and recent research has demonstrated that fluctuations in physiological variables are correlated with fluctuations in dFC during a stressor [Eisenbarth et al, 2016]. The vmPFC in particular is associated with task-related changes in variables indexing physiological arousal, such as heart rate [Eisenbarth et al., 2016; Young et al, 2017; Chang et al, 2013; Thayer et al, 2012]. Physiological responses, however, are also associated with emotional experience and behavior [Mauss et al., 2005], and, importantly, the strength of this relationship depends on the subjective intensity of emotions. Thus, it is not clear whether physiological arousal would be a nuisance variable that needs to be controlled in this type of experiment, or if it would be a variable of interest that is relevant to understanding the relationship between SET task engagement, its stress-inducing effects, and concurrent brain signals. Future investigations that measure concurrent physiological variables will be able to begin answering this important question.

Dynamic Functional Connectivity, the DCS, and the PARAFAC Decomposition

Synchronization between two or more signals may be caused by co-activation, (concurrent supra-threshold amplitude) [Tagliazucchi et al., 2016; Liu and Duyn, 2013; Amico et al, 2014], and by coordinated oscillations (coordinated rate of change), or by correlated noise in the signals. The DCS, developed for this study, as a filter does not protect against contamination in the signal by sources of noise. The DCS is particularly intended to identify synchronization in a wideband signal—if two wideband signals become dominated, even briefly, by the same component frequency (regardless of that frequency), then the DCS will detect it as synchronous. If the two wideband signals do not lock onto the same frequency, then the DCS will filter out rapid fluctuations stemming from the instantaneous frequency modulations of each signal. In addition, co-activation does not imply synchrony per se [see Di et al, 2015 for an example of co-activation versus synchronization], and oscillation synchrony is independent of activation thresholds. The DCS does not differentiate among these types of synchrony, and instead detects either type as contributing to dFC. However, it is likely that each type of synchronization uniquely contributes to information processing subserved by dFC, and future research efforts should disentangle them from each other to elucidate the possible mechanisms by which individual variability in dFC is related to cognition and behavior.

The PARAFAC decomposition used in this study successfully identified dFC brain networks that were related to individual differences in conscious emotional experience, but several characteristics of the model should be explored in future studies. For example, the PARAFAC model did not include constraints for non-negative factors but the factor loadings for the time and participant modes were unanimously non-negative. Also, preprocessing of the group dFC data did not include mean centering of the DCS tensor, nor did it include a dimensionality reduction step, such as principal components analysis (PCA) as is common in group analyses employing independent components analysis (ICA). The unanimously non-negative factors may be explained by the fact that the DCS was not mean centered, or it may be due to the symmetry of the two spatial modes. In addition, dimensionality reduction prior to PARAFAC decomposition may lead to improved model fit and should be explored in future applications. Finally, setting the rank parameter for the PARAFAC decomposition is not trivial. We employed the core consistency diagnostic on each individual participant's data to estimate the optimal rank of the model, however, it is possible that the group data is of higher (or lower) rank than the aggregate of individual participants' data, or that some of the networks are especially idiosyncratic and may contribute only noise to the model solution, as in the case of component 4 that was dominated by a participant with large head motion. Future research that applies the PARAFAC decomposition to group dFC tensor should explore or develop alternative methods for determining the rank of the full data set—those that can estimate the rank without the need to compute model solutions across a range of possible ranks would be most useful.

LIMITATIONS

This study has several limitations that impact its generalizability and utility in elucidating individual differences in stress and coping responses to psychological stressors.

First, an $N = 16$ is a small sample size on which to base conclusions regarding the human population at large, and this is further limited by the all-female sample. Future studies should include males and females from a much larger sample of the population to improve the generalizability of the results, and potentially identify gender differences in the neural correlates of stress and coping mechanisms. Second, the ratings of emotions used in this study were collected retrospectively, after the scan was over, and the threat-related and relief-related ratings were collected in succession without counterbalancing. This aspect of the study can be improved by recording continuous measures of affective valence and/or intensity throughout the scan, which would eliminate the need to collect two sets of ratings because changes in emotions could be related to SET and brain network events as they unfold in real time. A third limitation is the lack of physiological data, such as respiratory, cardiac and skin conductance activity, and the lack of data concerning cortisol responses. Inclusion of these data in future studies would provide a more complete picture of how multiple components of the stress response are coordinated with neural activity and vary across individuals. Finally, the short recovery period precludes analysis of rumination, which is an important component of how stress affects individuals after disengaging from the stressor. The post-stressor recovery scan period can be extended in future studies and data can be collected with experience sampling-type protocols [Van Calster et al., 2017] to probe the occurrence and contents of ruminative thoughts, and relate them to the neural underpinnings of individual differences in stress, and recovery and coping strategies.

SUMMARY

The dynamics of emotional processing in the brain are rich with information concerning the timing and duration, and resurgence of emotional experiences [Waugh et al, 2015]. In this study, participants were exposed to psychosocial threat while neural signals were recorded with fMRI, and subjective emotional intensity ratings were collected retrospectively after the scanning session. A dFC tensor was computed for each participant's whole-brain fMRI signals and the group dFC tensor was decomposed with PARAFAC. The participant loadings output by the PARAFAC model indicate individual differences in the strength of expression of the spatial network and its temporal dynamics reflected in the component. The main findings of this study indicate that the synchronization strength of stress-induced positive and negative emotion-related brain networks varies in relation to the subjective intensity of the experienced emotions, and that these networks fluctuate independently. In sum, these findings suggest that dFC of emotion-related networks may serve as a mechanism that generates individual differences in psychosocial stress, coping with stress, and recovering from stress. This study contributes to a growing literature that documents the importance of dFC, and specifically illustrates the importance of considering individual differences in dFC when investigating the network dynamics related to subjective emotional experiences.

ACKNOWLEDGMENTS

The authors thank Emily Dennis, Juliana Gonzales, Kalpa Bhattacharjee, Arkadiy Maksimovskiy, and Maria Lemus for their help in data collection and preparation. The authors also thank Paul Hamilton, Jutta Joormann, and Michael Chen for their help with the design of the original study on which these secondary analyses were based. The authors want to thank two anonymous reviewers for their insightful and constructive comments on earlier drafts of this manuscript.

REFERENCES

Amico E, Gomez F, Di Perri C, Vanhaudenhuyse A, Lesenfants D, Boveroux P, Bonhomme V, Brichart JF, Marinazzo D, Laureys S (2014): Posterior cingulate cortex-related co-activation patterns: A resting state fMRI study in propofol-induced loss of consciousness. PLoS One 9:e100012. doi: 10.1371/journal.pone.0100012.

Bader BW, Kolda TG (2015): MATLAB Tensor Toolbox Version 2.6. url: http://www.sandia.gov/~tgkolda/TensorToolbox/

Banks SJ, Eddy KT, Angstadt M, Nathan PJ, Phan KL (2007): Amygdala-frontal connectivity during emotion regulation. Soc Cogn Affect Neurosci 2:303–312.

Benjamini Y, Hochberg Y (1995): Controlling the false discovery rate: A practical and powerful approach to multiple testing. J R Stat Soc Ser B 57:289–300.

Bosch JA, de Geus EJC, Carroll D, Goedhart AD, Anane LA, van Zanten JJV, Helmerhorst EJ, Edwards KM (2009): A general enhancement of autonomic and cortisol responses during social evaluative threat. Psychosomat Med 71:877–885.

Braun U, Schafer A, Walter H, Erk S, Romanczuk-Sieferth N, Haddad L, Schweiger JL, Grimm O, Heinz A, Tost H, Meyer-Lindbergh A, Bassett DS (2015): Dynamic reconfiguration of frontal brain networks during executive cognition in humans. Proc Natl Acad Sci 112:11678–11683.

Bro R, Kiers HA (2003): A new efficient method for determining the number of components in parafac models. J Chemometrics 17:274–286.

Carroll JD, Chang J (1970): Analysis of individual differences in multidimensional scaling via N-way generalization of an Eckart-Young decomposition. Psychometrika 35:283.

Cavanaugh JF, Allen JJ (2008): Multiple aspects of the stress response under social evaluative threat: an electrophysiological investigation. Psychoneuroendocrinology 33:41–53.

Chang C, Glover G (2010): Time-frequency dynamics of resting-state brain connectivity measured with fmri. NeuroImage 50: 81–98.

Chang C, Metzger CD, Glover GH, Duyn JH, Heinze H, Walter M (2013): Assocaition between heart rate variability and fluctuations in resting-stte functional connectivity. NeuroImage 68: 93–104.

Costa T, Cauda F, Crini M, Tatu M, Celeghin A, de Gelder B, Tamietto M (2014): Temporal and spatial neural dynamics in the perception of basic emotions from complex scenes. Soc Cogn Affect Neurosci 9:1690–1703.

Cox RW (1996): AFNI: Software for analysis and visualization of functional magnetic resonance neuroimages. Comput Biomed Res 29:162–173.

Craddock RC, James GA, Holtzheimer PE, Hu X, Mayberg HS (2012): A whole brain fMRI atlas generated via spatially constrained spectral clustering. Hum Brain Mapp 33:1914–1928.

Cribben I, Wager TD, Lindquist MA (2013): Detecting functional connectivity change points for single-subject fMRI data. Front Comput Neurosci. doi: 10.3389/fncom.2013.00143.

Di X, Fu Z, Chan SC, Hung YS, Biswal BB, Zhang Z (2015): Task-related functional connectivity dynamics in a block-designed visual experiment. Front Hum Neurosci. doi: 10.3389/fnhum.2015.00543.

Dickerson SS (2008): Emotional and physiological responses to social-evaluative threat. Social Personal Psychol Compass 2: 1362–1378.

Dore BP, Weber J, Ochsner KN (2017): Neural predictors of decisions to cognitively control emotion. J Neurosci. doi: doi.org/10.1523/JNEUROSCI.2526-16.2016.

Eisenbarth H, Chang LJ, Wager TD (2016): Multivariate brain prediction of heart rate and skin conductance responses to social threat. J Neurosci 36:11987–11998.

Esslen M, Pasqual-Marqui RD, Hell D, Kochi K, Lehmann D (2004): Brain areas and time course of emotional processing. NeuroImage 21:1189–1203.

Feldman PJ, Cohen S, Lepore SJ, Matthews KA, Kamrack TW, Marsland AL (1999): Negative emotions and acute psychological responses to stress. Ann Behav Med 21:216–222.

Folkman S (2008): The case for positive emotions in the stress process. Anxiety Stress Coping 21:3–14.

Folkman S, Moskowitz JT (2000): Stress, positive emotion, and coping. Curr Directions Psychol Sci 9:115–118.

Gianaros PJ, Sheu LK, Matthews KA, Jennings JR, Manuck SB, Hariri AR (2008): Individual differences in stressor-evoked blood pressure reactivity vary with activation, volume, and functional connectivity to the amygdala. J Neurosci 28:990–999.

Glerean E, Salmi J, Lahnakoksi JM, Jaaskelainen IP, Sams M (2012): Functional magnetic resonance imaging phase synchronization as a measure of dynamic functional connectivity. Brain Connect 2:91–101.

Gonzalez-Castillo J, Bandettini PA (2017): Task-based dynamic functional connectivity: Recent findings and open questions. NeuroImage. in press, doi:10.1016/j.neuroimage.2017.08.006.

Handwerker DA, Roopichansingh V, Gonzalez-Castillo J, Bandettini PA (2012): Periodic changes in fMRI connectivity. NeuroImage 63:1712–1719.

Harshman RA (1970): Foundations of the PARAFAC procedure: model and conditions for an 'exploratory' multi-mode factor analysis. UCLA Working Papers in Phonetics, 16.

Helwig NE, Hong S (2013): A critique of tensor probabilistic independent component analysis: Implications and recommendations for multi-subject fMRI data analysis. J Neurosci Methods 213:263–273.

Hermans EJ, Henckens MJAG, Joels M, Fernandez G (2014): Dynamic adaptation of large-scale brain networks in response to acute stressors. Trends Neurosci 37:304–314.

Herry C, Bach DR, Esposito F, Di Salle F, Perrig WJ, Scheffler K, Luthi A, Seifritz E (2007): Processing of temporal unpredictability in human and animal amygdala. J Neurosci 27:5958–5966.

Hindriks R, Adhikari MH, Murayama Y, Ganzetti M, Mantini D, Logothetis NK, Deco G (2016): Can sliding-window correlations reveal dynamic functional connectivity in resting-state fMRI? NeuroImage 127:242–256.

Hot P, Sequeira H (2013): Time course of brain activation elicited by basic emotions. NeuroReport 24:898–902.

Huang NE, Shen Z, Long SR, Wu MC, Shih HH, Zheng Q, Yen NC, Tung CC, Liu HH (1998): The empirical mode decomposition and the Hilbert spectrum for nonlinear and nonstationary time series analysis. Proc R Soc Lond A 454:903–995. doi: 10.1098/rspa.1998.0193.

Hutchison RM, Womelsdorf T, Allen EA, Bandettini PA, Calhoun VD, Corbetta M, Della Penna S, Duyn JH, Glover GH, Gonzalez-Castillo J, Handwerker DA, Keilholz S, Kiviniemi V, Leopold DA, de Pasquale F, Sporns O, Walter M, Chang C (2013): Dynamic functional connectivity: Promises, issues, and interpretations. NeuroImage 80:360–378.

Jia H, Hu X, Deshpande G (2014): Behavioral relevance of the dynamics of the functional brain connectome. Brain Connect 4: 741–759.

Jin C, Lanka P, Rangaprakash D, Li L, Liu T, Hu X, Deshpande G (2017): Dynamic brain connectivity is a better predictor of PTSD than static connectivity. Hum Brain Mapp. doi: 10.1002/hbm.23676

Laumann TO, Snyder AZ, Mitra A, Gordon EM, Gratton C, Adeyemo B, Gilmore AW, Nelson SM, Berg JJ, Greene DJ, McCarthy JE, Tagliazucchi E, Laufs H, Schlaggar BL, Dosenbach NUF, Petersen SE (2016): On the stability of BOLD fMRI correlations. Cerebral Cortex.

Lazarus RS (1993): From psychological stress to the emotions: A history of changing outlooks. Annu Rev Psychol 44:1–21.

Leonardi N Van De Ville (2015): On spurious and real fluctuations of dynamic functional connectivity during rest. NeuroImage 104:430–436.

Leonardi N, Richiardi J, Gschwind M, Simioni S, Annoni J, Schluep M, Vuilleumier P, Van De Ville D (2013): Principal components of functional connectivity: A new approach to study dynamic brain connectivity during rest. NeuroImage 83:937–950.

Liegeois R, Ziegler E, Phillips C, Geurts P, Gomez F, Bahri MA, Yeo BTT, Soddu A, Vanhaudenhuvse A, Laureys S, Sepulchre R (2016): Cerebral functional connectivity periodically (de)synchronizes with anatomical constraints. Brain Struct Funct 221:2985–2997.

Liegeois R, Laumann TO, Snyder AZ, Zhou J, Yeo BTT (2017): Interpreting temporal fluctuations in resting-state functional connectivity. NeuroImage. in press: doi:10.1016/j.neuroimage.2017.09.012.

Lindquist KA, Wager TD, Kober H, Bliss-Moreau E, Barrett LF (2012): The brain basis of emotion: A meta-analytic review. Behav Brain Sci 35:121–143.

Liston C, McEwen BS, Casey BJ (2009): Psychosocial stress reversibly disrupts prefrontal processing and attentional control. Proc Natl Acad Sci 106:912–917.

Liu X, Duyn JH (2013): Time-varying functional network information extracted from brief instances of spontaneous brain activity. Proc Natl Acad Sci 110:4392–4397.

Mauss IB, Levenson RW, McCarter L, Wilhelm FH, Gross JJ (2005): The tie that binds? Coherence among emotion, experience, behavior and physiology. Emotion 5:175–190.

Mauss IB, Robinson MD (2009): Measures of emotion: A review. Cogn Emotion 23:209–237.

Moon SM, Lord RG (2006): Individual differences in automatic and controlled regulation of emotion and task performance. Hum Perform 19:327–356.

Mooneyham BW, Mrazek MD, Mrazek AJ, Mrazek KL, Phillips DT, Schooler JW (2017): States of mind: Characterizing the neural bases of focus and mind-wandering through dynamic functional connectivity. J Cogn Neurosci 29:495–506.

Morawetz C, Bode S, Baudewig J, Heekeren HR (2017): Effective amygdala-prefrontal connectivity predicts individual differences in successful emotion regulation. Soc Cogn Affect Neurosci 2017:569–585.

Morup M, Hansen LK (2009): Automatic relevance determination for multi-way models. J Chemometrics 23:352–363.

Motzkin JC, Phillipi CL, Wolf RC, Baskaya MK, Koenigs M (2015): Ventromedial prefrontal cortex is critical for the regulation of amygdala activity in humans. Biol Psychiatry 77:276–284.

Nikolau F, Orphanidou C, Papakyriakou P, Murphy K, Wise RG, Mitsis GD (2016): Spontaneous physiological variability modulates dynamic functional connectivity in resting-state functional magnetic resonance imaging. Phil Trans R Soc A 374:201508183.

Ong AD, Bergeman CS, Bisconti TL, Wallace KA (2006): Psychological resilience, positive emotions, and successful adaptation to stress later in life. J Personal Social Psychol 91:730–749.

Papalexakis EE, Faloutsos C (2015): Fast efficient and scalable Core Consistency Diagnostic for the parafac decomposition for big sparse tensors. 2015 IEEE International Conference on Acoustics, Speech and Signal Processing (ICASSP). doi: 10.1109/ICASSP.2015.7179011.

Phelps EA, Ledoux JE (2005): Contributions of the amygdala to emotion processing: From animal models to behavior. Neuron 48:175–187.

Ponce-Alvarez A, Deco G, Hagmann P, Romani GL, Mantini D, Corbetta M (2015): Resting-state temporal synchronization networks emerge from connectivity topology and heterogeneity. PLoS Comput Biol 11:e1004100. doi: 10.1371/journal.pcbi.1004100.

Preti MG, Bolton TAW, Van De Ville D (2017): The dynamic functional connectome: State of the art and perspectives. NeuroImage

Pruessner JC, Dedovic K, Khalili-Mahani N, Engert V, Pruessner M, Buss C, Renwick R, Dagher A, Meaney MJ, Lupien S (2008): Deactivation of the limbic system during acute psychosocial stress: Evidence from positron emission tomography and functional magnetic resonance imaging studies. Biol Psychiatry 63:234–240.

Qin S, Hermans EJ, van Marle HJF, Luo J, Fernandez G (2009): Acute psychological stress reduces working memory-related activity in the dorsolateral prefrontal cortex. Biol Psychiatry 66:25–32.

Rafaeli E, Rogers GM, Revelle W (2007): Affective synchrony: Individual differences in mixed emotions. Personal Social Psychol Bull 33:915–932.

Roy M, Shohamy D, Wager TD (2012): Ventromedial prefrontal-subcortical systems and the generation of affective meaning. Trends Cogn Sci 16:147–156.

Scheibe S, Blanchard-Fields F (2009): Effects of regulating emotions on cognitive performance: What is costly for young adults is not so costly for older adults. Psychol Aging 24: 217–223.

Schultz A, Vogele C (2015): Interoception and stress. Front Psychol 6:993. doi: 10.3389/fpsyg.2015.00993

Seeley WW, Menon V, Schatzberg AF, Keller J, Glover GH, Kenna H, Reiss AL, Greicius MD (2007): Dissociable intrinsic connectivity networks for salience processing and executive control. J Neurosci 27:2349–2356.

Senden M, Reuter N, van den Heuvel MP, Goebel R, Deco G (2016): Cortical rich club regions can organize state-dependent functional network formation by engaging in oscillatory behavior. NeuroImage

Shakil S, Lee C, Keilholz SD (2016): Evaluation of sliding window correlation performance for characterizing dynamic functional connectivity. NeuroImage 133:111–128.

Siegel JS, Mitra A, Laumann TO, Seitzman BA, Raichle M, Corbetta M, Snyder AZ (2017): Data quality influences observed links between functional connectivity and behavior. Cereb Cortex 27:4492–4502.

Smith TW, Nealey JB, Kircher JC, Limon JP (1997): Social determinants of cardiovascular reactivity: Effects of incentive to exert influence and evaluative threat. Psychophysiology 34:65–73.

Soares JM, Sampaio A, Ferreira LM, Santos NC, Marques P, Marques F, Palha JA, Cerqueira JJ, Sousa N (2013): Stress impact on resting state brain networks. PLoS One 8:e66500. doi: 10.1371/journal.pone.0066500

Tagliazucchi E, Siniatchkin M, Laufs H, Chialvo DR (2016): The voxel-wise functional connectome can be efficiently derived from co-activations in a sparse spatio-temporal point-process. Front Neurosci 10:381. doi: 10.3389/fnins.2016.00381.

Telesford QK, Lynall M, Vettel J, Miller MB, Grafton ST, Bassett DS (2016): Detection of functional brain network reconfiguration during task-driven cognitive states. NeuroImage 142:198–210.

Terasawa Y, Fukushima H, Umeda S (2013): How does interoceptive awareness interact with the subjective experience of emotion? An fMRI study. Hum Brain Mapp 34:598–612.

Thayer JF, Ahs F, Fredrickson M, Solers JJ, Wager TD (2012): A meta-analysis of heart rate variability and neuroimaging studies. Neurosci Biobehav Rev 36:747–756.

Timmerman ME, Kiers HAL (2000): Three-mode principal components analysis: Choosing the numbers of components and sensitivity to local optima. Br J Math Stat Psychol 53:1–16.

Tugade MM, Fredrickson BL (2004): Resilient individuals use positive emotions to bounce back from negative emotional experiences. J Personal Social Psychol 86:320–333.

Ulrich-Lai YM, Herman JP (2009): Neural regulation of endocrine and autonomic stress response. Nat Rev Neurosci 10: 397–409.

Urry HL, van Reekum CM, Johnstone T, Kalin NH, Thurow ME, Schaefer HS, Jackson CA, Frye CJ, Greischer LL, Alexander AL, Davidson RJ (2006): Amygdala and ventromedial prefrontal cortex are inversely coupled during regulation of negative affect and predict the diurnal pattern of cortisol secretion among older adults. J Neurosci 26:4415–4425.

Vaisvaser S, Lin T, Admon R, Podlipsky I, Greenman Y, Stern N, Fruchter E, Wald I, Pine DS, Tarrasch R, Bar-Haim Y, Hendler T (2013): Neural traces of stress: Cortisol related sustained enhancement of amygdala-hippocampal functional connectivity. Front Hum Neurosci 7. doi: 10.3389/fnhum.2013.00313

Van Calster L, D'Argembeau A, Salmon E, Peters F, Majerus S (2017): Fluctuations of attentional networks and default mode network during the resting state reflect variations in cognitive states: Evidence from a novel resting-state experience sampling method. J Cogn Neurosci 29:95–113.

Van der Werff SJA, van den Berg SM, Pannekoek JN, Elzinga BM, van der Wee NJA (2013): Neuroimaging resilience to stress: A review. Front Behav Neurosci doi: 10.3389/fnbeh.2013.00039

van Marle HJF, Hermans EJ, Qin S, Fernandez G (2010): Enhanced resting-state connectivity of amygdala in the immediate aftermath of acute psychological stress. NeuroImage 53:348–354.

Veer IM, Oei NYL, Spinhoven P, van Buchem M, Elzinga BM, Rombouts SARB (2012): 57:1534–1541. Beyond acute social stress: increased functional connectivity between amygdala and cortical midline structures. NeuroImage,

Verduyn P, Delvaux E, Van Coillie H, Tuerlinckx F, Van Mechelen I (2009): Predicting the duration of emotional experience: Two experience sampling studies. Emotion 9:83–91.

Verduyn P, Van Mechelen I, Frederix E (2012): Determinants of shape of emotion intensity profiles. Cogn Emotion 26: 1486–1495.

Wager TD, Waugh CE, Lindquist M, Noll DC, Frederickson BL, Taylor SF (2009a): Brain mediators of cardiovascular response to social threat, Part I: Reciprocal dorsal and ventral subregions of the medial prefrontal cortex and heart-rate reactivity. NeuroImage 47:821–835.

Wager TD, van Ast VA, Hughes BL, Davidson ML, Lindquist MA, Ochsner KN (2009b): Brain mediators of cardiovascular response to social threat, Part II: Prefrontal-subcortical pathways and relationship with anxiety. NeuroImage 47: 836–851.

Waugh CE, Wager TD, Fredrickson BL, Noll DC, Taylor SF (2008): The neural correlates of trait resilience when anticipating and recovering from threat. Soc Cogn Affect Neurosci 3: 322–332.

Waugh CE, Hamilton JP, Chen MC, Joormann J, Gottlib IH (2012): Neural temporal dynamics of stress in comorbid major depressive disorder and social anxiety disorder. Biol Mood Anxiety Disord 2:11. doi:10.1186/2045-5380-2-11.

Waugh CE, Panage S, Mendes WB, Gottlib IH (2010): Cardiovascular and affective recovery from anticipatory threat. Biol Psychol 84:169–175.

Waugh CE, Shing EZ, Avery BM (2015): Temporal dynamics of emotional processing in the brain. Emotion Rev 7:323–329.

Wheelock MD, Harnett NG, Wood KH, Orem TR, Granger DA, Mrug S, Knight DC (2016): Prefrontal cortex activity is associated with biobehavioral components of the stress response. Front Hum Neurosci. doi: 10.3389/fnhum.2016.00583

Xia M, Wang J, He Y (2013): BrainNet viewer: A network visualization tool for human brain connectomics. PLoS One 8:e68910. doi: 10.1371/journal.pone.0068910

Xie H, Calhoun V, Gonzalez-Castillo J, Damaraju E, Miller R, Bandettini P, Mitra S (2017): Whole-brain connectivity dynamics reflect both task-specific and individual-specific modulation: A multi-task study. NeuroImage doi: dx.doi.org/10.1016/j.neuroimage.2017.05.050

Young CB, Raz G, Everaerd D, Beckmann CF, Tendolkar I, Hendler T, Fernandez G, Hermans EJ (2017): Dynamic shifts in large-scale brain network balance as a function of arousal. J Neurosci 37:281–290.

Zalesky A, Fornito A, Cocchi L, Gollo LL, Breakspear M (2014): Time-resolved resting-state brain networks. Proc Natl Acad Sci 111:10341–10346.